

Detection of quantum well induced single degenerate-transition-dipoles in ZnO nanorods

Siddharth Ghosh¹, Moumita Ghosh^{2,3,4}, Michael Seibt⁴, G Mohan Rao³*

¹III. Institute of Physics, Georg-August-Universität-Göttingen, Friedrich-Hund-Platz 1,
37075 Göttingen, Germany.

²Centre for Nano Science and Engineering, Indian Institute of Science, Bangalore 560012,
India.

³Instrumentation and Applied Physics, Indian Institute of Science, Bangalore 560012,
India.

⁴IV. Institute of Physics, Georg-August-Universität-Göttingen, Friedrich-Hund-Platz 1,
37075 Göttingen, Germany.

*Corresponding email addresses:

M. G. at ghoshiisc@gmail.com and S. G. at siddharth.ghosh@phys.uni-goettingen.de

Contents:

- 1. Synthesis of ZnO nanorods**
- 2. Ferroelectric characterisation**
- 3. Defocused imaging setup**
- 4. Sample preparation for defocused imaging**
- 5. Multi-dimensional dipole modeling**
- 6. Photoluminescence properties of Native and QW ZnO nanorod**

7. X-ray diffraction confirming zinc blend and wurtzite crystal structure

8. Energy dispersive spectroscopy under HRTEM

1. Synthesis of ZnO nanorods.

Sol-gel technique has been used to synthesise defect engineered ZnO nanorods^{S1}. The nanorods are grown on 30 nm seed layer of ZnO thinfilm. The substrate used here was (100) p-type silicon wafer coated with titanium and platinum with thinfilm thickness of 15 nm and 200 nm, respectively. The ZnO nanorods have height of 500-550 nm and width of 50 nm.

2. Ferroelectric characterisation - Polarisation-electric field loop (P-E loop).

In house modified Sawyer Tower circuit was built and a TDS1000-EDU Tektronix oscilloscope. The Sawyer Tower circuit has been modified by incorporating a compensation network along with an attenuating network. This prevents flow of high leakage current through the desired sample and nullifies its effect on output polarisation. The platinum-titanium layer was used as bottom electrode and for top electrode aluminium was deposited with metal mask^{S2}.

3. Defocused imaging setup.

The defocused images were obtained with an Olympus IX71 widefield optical microscope with certain in-house modification. The total magnification used was of 160×. An oil immersion 100× Olympus TIRF objective lens was used. The numerical aperture of the objective was 1.49. A camera controlled CW Omicron Phoxx 488-60 laser was used for 488 nm excitation wavelength. The laser was pulsed based on the exposure time of the

camera. Andor iXon Ultra 897 high speed EMCCD camera has captured the defocused pattern. At the detection path a Semrock 525 nm narrow band pass filter was used. The PI fork (P-725.2CD) has precisely allowed us to displace from the focal plane.

4. Sample preparation for defocused imaging.

Menzel 150 μm thick coverslip was used. The coverslips were ultrasonicated in acetone immersion bath for 15 min and thereafter air plasma cleaned for another 20 min. The cleaning protocol allows us to reduce background signal from glass to capture high signal to noise ratio of single emitters. The pristine coverslip and the vertical ZnO nanorod containing silicon substrates were came into contact inside a class 100 clean room environment. Then, they were vacuum bonded. This bonding is reversible.

5. Multi-dimensional dipole modelling.

The thickness of the glass below the emitters was considered to be infinity with refractive index of 1.52. The thickness of the ZnO nanorod (550 nm) was considered as thickness emitter's layer with refractive index 2.06. On top of the nanorod 30 nm seed layer of ZnO had same refractive index as 2.06. The titanium and platinum layer with respective thickness of 15 nm and 200 nm were considered to have refractive index of 1.76 and 1.93, respectively. The top most layer was p-type silicon substrate, where refractive index was 4.35. The thickness of this layer was considered as infinity.

Fig.S1 schematically represent the optics working behind defocused imaging. Here, the degenerate dipole has considered being the super position of three dipoles (x, y and z). By displacing the optics, one can capture the defocused image of the transition dipole on the EMCCD plane. In short the focal point has to be displaced along the optical axis as

shown by displacing the EMCCD plane in Fig.S1. However, the easiest approach is to displacing the objective lens. The angular distribution of dipole depends on the electrodynamic interaction at the interface as shown in Fig.S2 (2), where a vertical component of the 3D dipole is interacting with a air/glass interface. Here the angular distribution of the oscillating dipole is simply defined by two particular angles, θ and ϕ . So, the amplitude of the electric field will be:

$$E(\theta, \phi) = \sin \psi [t_s E_s''(\theta) \sin \phi + t_p E_p''(\theta) \cos \phi] + t_p E_p^\perp(\theta) \cos \psi$$

Here, ψ is the polar angle and t_p and t_s are orthogonal unit vectors. Now, considering transmission coefficient of Fresnel for p and s waves, distance of the dipole from the glass/air interface and the refractive indices of the both the media one can easily define the $E_p^\perp(\theta)$, $E_p''(\theta)$ and $E_s''(\theta)$ as shown by Enderlein et al.,^{S3}.

As we have degenerate or 3D dipole, so in our case the dipole has three vector component defining three different dipoles and their superposition on a single point. Therefore, if one has defined all three dipoles considering all the Euler angles as aforementioned, it is straightforward to calculate their superposition^{S4}. As we have mentioned in our letter that when we are considering superposition of three dipoles, it is important to define their intensity distribution. Considering their intensity as I_x , I_y and I_z for x , y and z dipoles, respectively, and their ratio of intensities as κ and η , the coupled intensity distribution^{S4} is proportional to

$$P = \kappa I_z + (1 - \kappa) [I_y (1 + \eta) / 2 + I_x (1 - \eta) / 2]$$

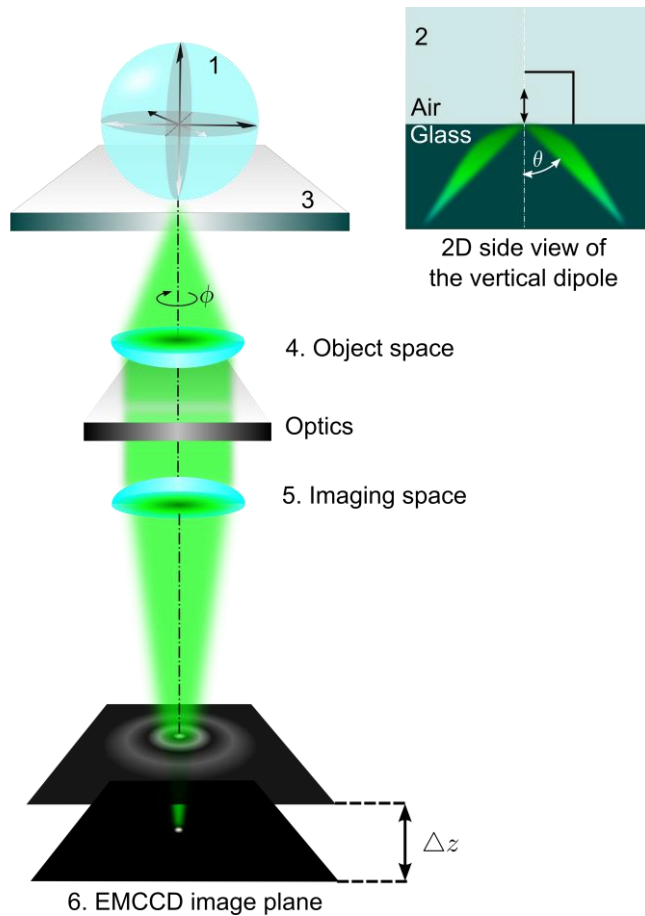


Fig.S1. Geometric schematic of defocused imaging. A three dimensional transition dipole or in other word a degenerate transition dipole is imaged onto a EMCCD plane by moving the optics along the optical axis in the direction away from the dipole or towards the EMCCD. This generates the interference pattern on the emitting dipole containing the orientation information. Here the dipole is considered to be the superposition of the three different dipoles as an approximation of the 3D dipole. The vertical component of the dipole's electrodynamic interaction with glass-air interface is shown from the side view (2), where the angular distribution of emission is dependent on two particular angles θ and ϕ .

6. Photoluminescence of ZnO.

If pure ZnO is excited with 325 nm UV laser, it emits with sharp peak near 365 nm. In our case also, we observe from the emission spectra as shown in Fig.S2 (a) that the ZnO nanorods exhibits same emission peak confirming the presence of ZnO. However, no single dipole could be observed at this emission wavelength. On the other hand, the photoluminescence image of the ZnO nanorods at 525 nm wavelength shows distinct single dipoles. At this wavelength we perform the defocused imaging to obtain the emission pattern of the dipole. Fig.S2(b) was captured using fast and synchronised exposure of the laser and the EMCCD at 200 ms. The fast blinking behaviour the ZnO nanorods allows to capture the temporally non-coherent emission of the single dipoles generated from the quantum well of the nanorods. Fig.S2 (c) shows a profile intensity plot from (b) with maximum signal to noise ratio of 2. The transmission wavelengths of the optical filter placed in the emission path are plotted in Fig.S2(d). Where the nanorods were excited with 488 nm laser and emission were captured in the wavelength window of 500 to 550 nm.

Overlapping emission dipole pattern is a critical issue of defocused imaging. Therefore, close spatial density of emitter should be avoided. As observed in the SEM images (Fig. S2 (a)) of ZnO nanorods that they are very closely packed with around 100 nm spatial distance from each other. This kind of spatial distance is considered to be a very uniform and good quality nanorod thin film for various applications considering specifically for measuring electrical behaviour. However, this spatial density was disadvantageous for defocused imaging because of capturing high quality emission dipole pattern with long exposure of laser and camera and thereby capturing all the dipoles

irrespective blinking behaviour and finally a sum image of their overlapped patterns. As shown in Fig.S3, it is hard to distinguish the patterns when the nanorods are closely space.

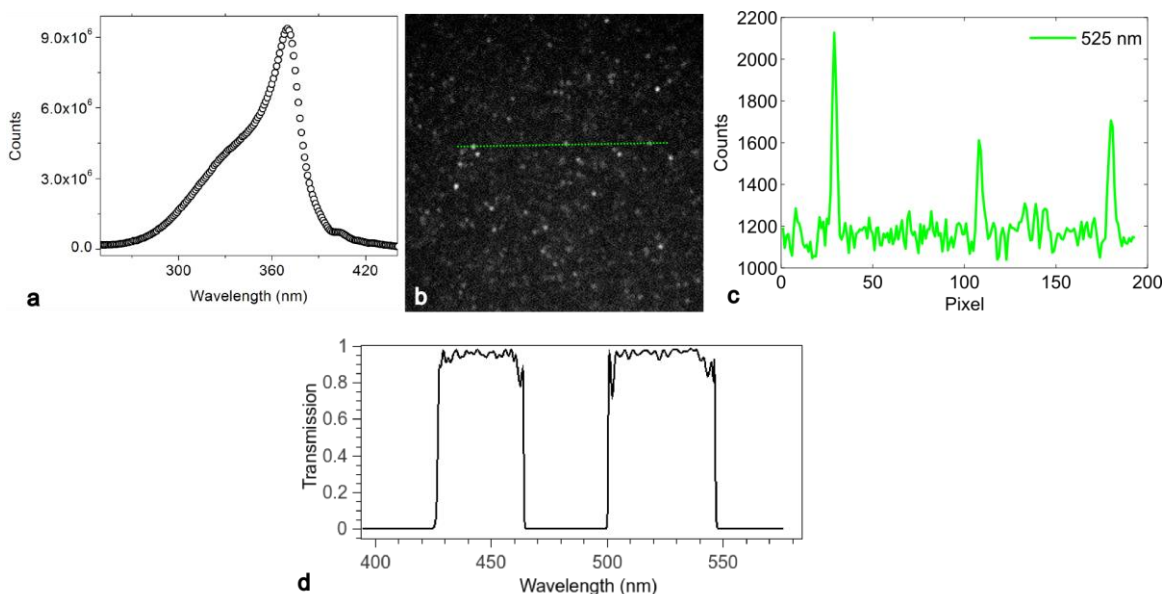


Fig.S2. (a) Innate photoluminescence of pure ZnO or considered as identifying emission peak of ZnO at 365 nm. (b) PL image at 525 nm emission wave length captured at very fast exposure utilising the blinking behaviour, (c) profile plot of the green line from (b) showing the signal to noise ratio of ZnO nanorods. (d) Transmission wavelengths of the filter used in the emission path.

A long exposure image shown in Fig.S3(a) shows the overlapped emission pattern and therefore a blurry image. On the other hand, keeping the blinking behaviour in to mind and short exposure generates a lossy image in a dense area as shown in Fig.S3(b)-(d). Although lossy but the emission dipole pattern are consistent everywhere - confirming that all the nanorods are having same kind of degenerate dipole. One can always say that there are multiple dipoles and thereby we are capturing average dipole pattern. On the contrary, it has to be taken into account that the dipole pattern are always same even in very less

densely spaced areas as shown in the letter. It is to be mentioned that wherever we have captured the emission dipole pattern we have found the same pattern and supported by many earlier antibunching studies confirm that they have single dipoles in ZnO nanorods.

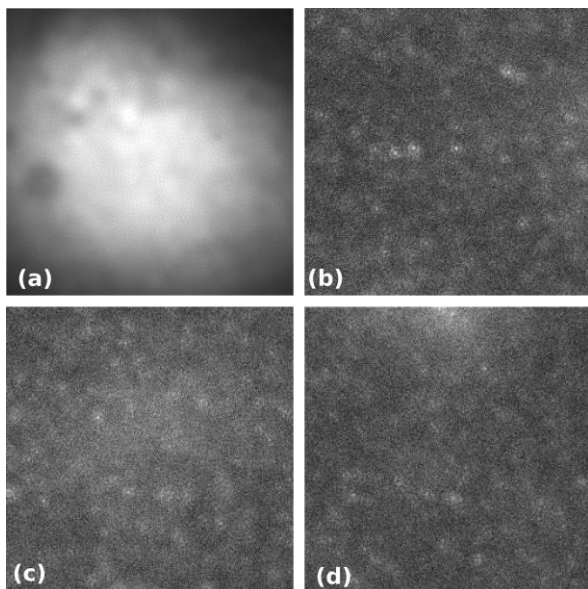


Fig.S3. Spatial density of ZnO nanorods growth matters for defocused imaging. (a) a slight defocusing of a very densely grown ZnO nanorods with spatial packing of around 100 nm hardly allows to discrete defocused pattern from single ZnO nanorods/single dipoles (b) – (d) shows another areas with slightly densely grown area compare to (a) however the spatial sparsity is not enough to distinguish clear patterns.

7. X-Ray Diffraction – Wurtzite and Stacking Fault

X-ray diffraction (XRD) spectroscopy was carried out on ZnO nanorod as shown in Fig.S4. The total XRD spectra is shown in Fig.S4(a) where the peak near 70° is due to the silicon substrate on which the nanorods were grown. Fig.S4(b) confirms that the ZnO nanorods has wurtzite crystallinity. A peak near 44.7° says that the the nanorods have some amount of zinc blend crystallinity (Fig.S4(c)). The peak here is very tiny and agrees well with the

HRTEM that percentage of zinc blend basal stacking fault per nanorod is around one which in turns compare to wurtzite peak will be very small percentage in total.

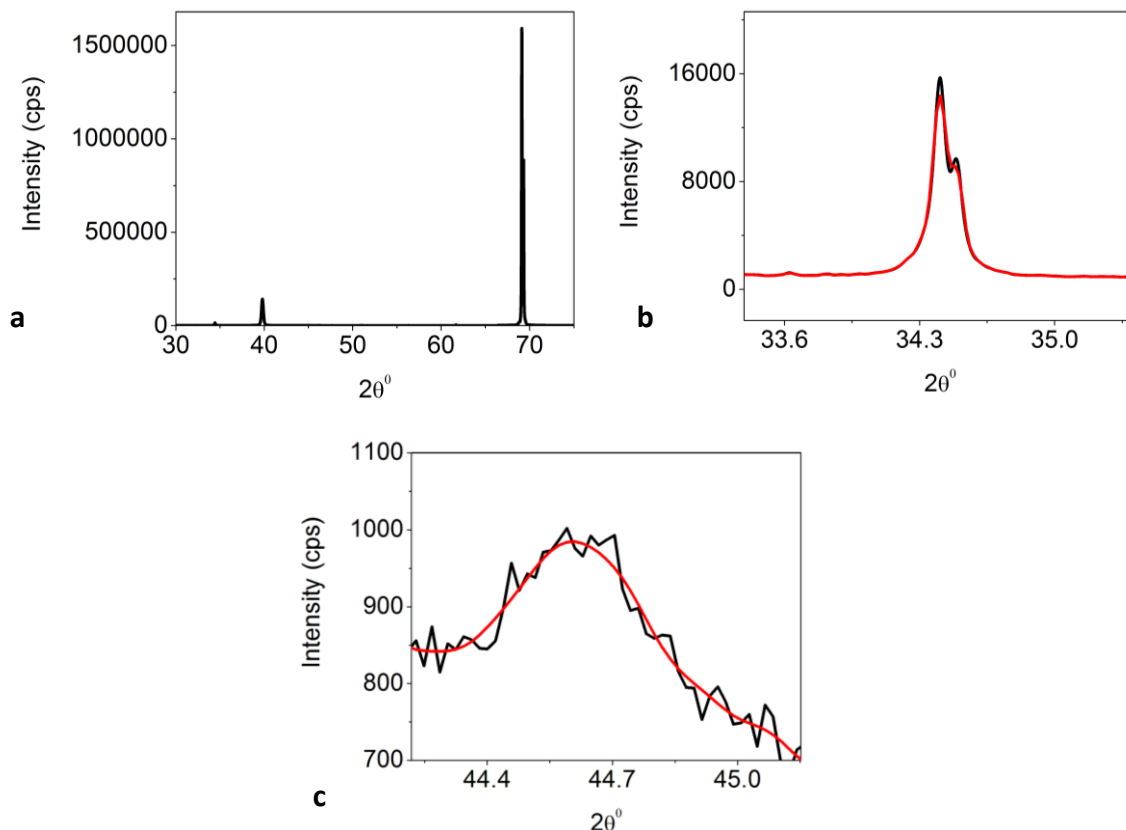


Fig. S4. XRD spectra showing presence of wurtzite and zinc blend crystallinity. (a)

shows complete spectra of ZnO nanorods. (b) The peak near 34.5° corresponds to wurtzite nature of the ZnO nanorod with very high signal to noise ratio^{S2}. (c) Presence of stacking fault with zinc blend crystallinity is also observed from the peak at 44.7° ^{S2,S5}, the signal to noise ratio is very low due to its very small percentage per nanostructure as HRTEM shows one basal stacking fault with zinc blend crystal structure per nanorod.

8. Energy dispersive spectroscopy under HRTEM

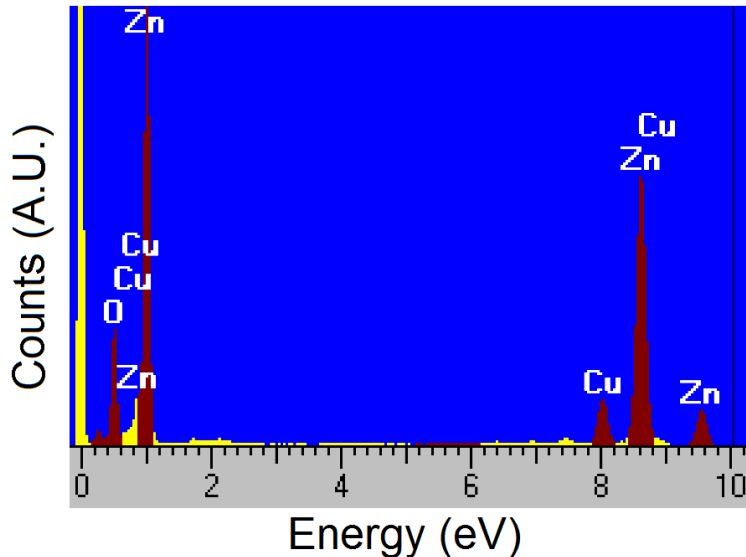


Fig. S5. Energy dispersive spectra under HRTEM on a single ZnO nanorod showing presence of zinc and oxygen atoms and no other elements. The copper peaks are from the background of TEM grid

REFERENCES

- S1. Ghosh, M. & Rao, G. M. Growth mechanism of ZnO nanostructures for ultra-high piezoelectric d_{33} coefficient. *Mater. Express* **3**, 319-327 (2013)
- S2. Ghosh, M.; Seibt, M.; Rao, K. Y.; Ghosh, S.; Peretzki, P.; Rao, G. M. Stacking fault in undoped ultra-high piezoelectric ZnO nanorod: HRTEM investigation along with electron beam effect. Ferroelectric-ultrahigh-piezoelectric undoped ZnO nanorod with stacking fault. *Submitted*.

S3. Enderlein, J.; Gregor, I., Ruckstuhl, T. Imaging properties of supercritical angle fluorescence optics. *Opt. Express.* **19**, 8011-18 (2011).

S4. Patra, D., Gregor, I., Enderlein J. & Sauer M. Defocused imaging of quantum dot angular distribution of radiation. *Appl. Phys. Lett.* **87**, 101103 (2005).

S5. Ashrafi, A. B. M. A.; Ueta, A.; Avramescu, A.; Kumano, H.; Suemune, I., Ok, Y. W.; Seong, T. Y. Growth and characterization of hypothetical zinc-blende ZnO films on GaAs(001)substrates with ZnS buffer layers. *Appl. Phys. Lett.* **76**, 550 (2000).